

AperTO - Archivio Istituzionale Open Access dell'Università di Torino

Depth of formation of super-deep diamonds: Raman barometry of CaSiO₃-walstromite inclusions

This is the author's manuscript

Original Citation:

Availability:

This version is available <http://hdl.handle.net/2318/1656157> since 2018-05-30T15:23:23Z

Published version:

DOI:10.2138/am-2018-6184

Terms of use:

Open Access

Anyone can freely access the full text of works made available as "Open Access". Works made available under a Creative Commons license can be used according to the terms and conditions of said license. Use of all other works requires consent of the right holder (author or publisher) if not exempted from copyright protection by the applicable law.

(Article begins on next page)

Depth of formation of super-deep diamonds: Raman barometry of CaSiO₃-walstromite inclusions

CHIARA ANZOLINI^{1,*}, MAURO PRENCIPE², MATTEO ALVARO³, CLAUDIA ROMANO⁴, ALESSANDRO VONA⁴,
SOFIA LORENZON¹, EVAN M. SMITH⁵, FRANK E. BRENKER⁶, AND FABRIZIO NESTOLA¹

¹Department of Geosciences, University of Padova, Via G. Gradenigo 6, 35131 Padova, Italy

²Department of Earth Sciences, University of Torino, Via Valperga Caluso 35, 10125 Torino, Italy

³Department of Earth and Environmental Sciences, University of Pavia, Via Ferrata 1, 27100 Pavia, Italy

⁴Department of Sciences, University of Roma Tre, Largo S. Leonardo Murialdo 1, 00146 Roma, Italy

⁵Gemological Institute of America, 50 W 47th Street, New York, New York, 10036 U.S.A.

⁶Geoscience Institute, Nanogeoscience, Goethe University, Altenhöferallee 1, 60438 Frankfurt am Main, Germany

ABSTRACT

“Super-deep” diamonds are thought to have a sub-lithospheric origin (i.e., below ~300 km depth) because some of the mineral phases entrapped within them as inclusions are considered to be the products of retrograde transformation from lower-mantle or transition-zone precursors. CaSiO₃-walstromite, the most abundant Ca-bearing mineral inclusion found in super-deep diamonds, is believed to derive from CaSiO₃-perovskite, which is stable only below ~600 km depth, although its real depth of origin is controversial. The remnant pressure (P_{inc}) retained by an inclusion, combined with the thermoelastic parameters of the mineral inclusion and the diamond host, allows calculation of the entrapment pressure of the diamond-inclusion pair. Raman spectroscopy, together with X-ray diffraction, is the most commonly used method for measuring the P_{inc} without damaging the diamond host.

In the present study we provide, for the first time, a calibration curve to determine the P_{inc} of a CaSiO₃-walstromite inclusion by means of Raman spectroscopy without breaking the diamond. To do so, we performed high-pressure micro-Raman investigations on a CaSiO₃-walstromite crystal under hydrostatic stress conditions within a diamond-anvil cell. We additionally calculated the Raman spectrum of CaSiO₃-walstromite by ab initio methods both under hydrostatic and non-hydrostatic stress conditions to avoid misinterpretation of the results caused by the possible presence of deviatoric stresses causing anomalous shift of CaSiO₃-walstromite Raman peaks. Last, we applied single-inclusion elastic barometry to estimate the minimum entrapment pressure of a CaSiO₃-walstromite inclusion trapped in a natural diamond, which is ~9 GPa (~260 km) at 1800 K. These results suggest that the diamond investigated is certainly sub-lithospheric and endorse the hypothesis that the presence of CaSiO₃-walstromite is a strong indication of super-deep origin.

Keywords: Diamond, inclusion, CaSiO₃-walstromite, micro-Raman spectroscopy, ab initio methods, elastic geobarometry

INTRODUCTION

Diamonds and the mineral inclusions that they trap during growth provide a unique window on the deep Earth. A small portion (~6%) of diamonds (Stachel and Harris 2008) are interpreted to crystallize between 300 and 800 km depth (Harte 2010) because some of the inclusions entrapped are considered to be the products of retrograde transformation from lower-mantle or transition-zone precursors. However, in many cases undisputed evidence of these purported high-pressure precursors as inclusions in diamonds is lacking, and, consequently, their real depth of origin has been proven only in rare cases (e.g., Brenker et al. 2002; Pearson et al. 2014). Most so-called “super-deep diamonds” contain mainly walstromite-structured CaSiO₃ (hereafter CaSiO₃-walstromite), ferropericlase [(Fe,Mg)O], enstatite

(MgSiO₃), and jeffbenite [(Mg,Fe)₃Al₂Si₃O₁₂], a tetragonal phase with garnet-like stoichiometry previously known by the acronym TAPP (see Nestola et al. 2016), and it is through the study of these mineral phases that the depth of formation of super-deep diamonds can be retrieved.

CaSiO₃-walstromite is the dominant Ca-bearing phase in super-deep diamonds (Joswig et al. 1999), and in almost all cases it is considered the product of back transformation from CaSiO₃-perovskite, which is stable only below ~600 km depth within the regular high-pressure assemblage of peridotitic/eclogitic mantle rocks (Frost 2008; Kaminsky 2012). However, there is compelling evidence that at least some CaSiO₃-walstromite originate within the upper mantle (Brenker et al. 2005; Anzolini et al. 2016), although this would require a substantial change in the source rock chemistry. Assuming peridotitic/eclogitic mantle chemistries, CaSiO₃-perovskite is the main Ca-host in the lower mantle (Ringwood 1991), but is also present in the

* E-mail: chiara.anzolini@phd.unipd.it

lowermost transition zone, where it exsolves from majoritic garnet at pressures greater than 20 GPa (Irifune and Ringwood 1987). Nevertheless, there are currently no reliable literature data on the exact pressure at which CaSiO_3 inclusions originally crystallize and therefore no valid evidence whether or not each CaSiO_3 -walsstromite derives from CaSiO_3 -perovskite.

Single-inclusion elastic barometry, a method recently improved by Angel et al. (2014a, 2014b, 2015a, 2015b), allows us to estimate the pressure and temperature conditions of entrapment for an inclusion within a diamond by knowing its residual pressure (P_{inc}), measured while the host is at ambient conditions, and the thermoelastic parameters of the mineral inclusion and the diamond host. In principle, the P_{inc} sustained by an inclusion while still entrapped within a diamond can be determined mainly in two ways: (1) by comparing the unit-cell volume of the inclusion before and after release from its host; (2) by comparing the Raman spectrum of the inclusion still trapped within the diamond and the Raman spectrum of the same mineral phase at room pressure. The first method requires inclusions large enough to be analyzed by single-crystal X-ray diffraction, but large inclusions are more likely to fracture the surrounding host during exhumation (Van der Molen and Van Roermund 1986; Artioli et al. 2008), and therefore their internal pressure is largely released. The second method allows to analyze tiny inclusions, which commonly preserve higher internal pressures, and, on the other hand, to prevent the host-inclusion system from destruction or damages. The host-inclusion system integrity preserves information about both the pressure exerted by the diamond on the inclusion and the relationships between the two, which may provide further details on the diamond-inclusion growth mechanisms (e.g., crystallographic orientation relationships, CORs; Nestola et al. 2014, 2017; Angel et al. 2015b; Milani et al. 2016).

In this light, we have determined experimentally the pressure-induced shift of Raman peaks for a synthetic CaSiO_3 -walsstromite up to 7.5 GPa under hydrostatic conditions to obtain a calibration system that enables us to determine the P_{inc} of a CaSiO_3 -walsstromite inclusion without breaking the diamond host. However, the effect of the elastic anisotropy of the host and the inclusion and the effect of a deviatoric stress field on the stress state of the inclusion arising from the absence of fluids at the interface between diamond and inclusion (see Nimis et al. 2016) are still unknown. Therefore, to prevent any misinterpretation of our results in terms of Raman peak shifts we calculated the Raman spectrum of CaSiO_3 -walsstromite by ab initio methods both under hydrostatic and non-hydrostatic conditions. Last, we estimated the entrapment pressure of a CaSiO_3 -walsstromite inclusion found in a diamond by single-inclusion elastic barometry.

EXPERIMENTAL METHODS

Samples

The single CaSiO_3 -walsstromite crystal, whose longest dimension is 40 μm , used for the high-pressure Raman investigations came from the experimental batch of Gasparik et al. (1994), synthesized at 2000 K and 9 GPa.

The diamond investigated in this study (Fig. 1a) was a 2.70-carat oval cut Type-II diamond. The inclusion investigated (Fig. 1b) was a CaSiO_3 -walsstromite, identified by comparison with Raman spectra reported by Nasdala et al. (2003) and Brenker et al. (2005, 2007).

Experimental in situ calibration of CaSiO_3 -walsstromite Raman spectra at high pressure

The ambient-pressure Raman spectrum of the synthetic single crystal of CaSiO_3 -walsstromite was collected with a Thermo-Scientific DXR Raman Microscope using a green solid-state laser (532 nm) as excitation source at the Department of Geosciences, University of Padova. The analyses were performed using a 50 \times long working distance (LWD) objective with $\sim 2.5 \text{ cm}^{-1}$ spectral resolution and 1 μm spatial resolution at 10 mW of power. The Raman system was set with 900 lines/mm grating and a 25 μm pinhole. Spectra were recorded in the frequency range extending from 100 to 3500 cm^{-1} ; to maximize the signal-to-noise ratio, each spectrum was collected 10 times using an exposure time of 20 s, and then merged together at the end of the acquisition. The instrument was calibrated by using the calibration tool provided by Thermo-Scientific.

The high-pressure Raman spectra were collected at the Department of Sciences, University of Roma Tre, with a Horiba LabRam HR micro-Raman spectrometer equipped with a green solid-state laser (532 nm) focused through a 20 \times LWD objective. A ETH diamond-anvil cell with 600 μm size culets was loaded with the crystal of CaSiO_3 -walsstromite and a 4:1 mixture of methanol:ethanol as pressure-transmitting medium. Pressure was determined by the calibrated shift of the R_1 ruby fluorescence band (Mao et al. 1986). The spatial resolution was $\sim 1 \mu\text{m}$ and the spectral resolution was 0.3 cm^{-1} . For the ruby, optical filters were employed to achieve $\sim 1 \text{ mW}$ at the sample surface; the Raman system was set with 1800 lines/mm grating, exposure time 1 s (3 times), confocal hole of 300 μm and slit of 200 μm . For the CaSiO_3 -walsstromite, optical filters were employed to achieve $\sim 50 \text{ mW}$ at the sample surface; the Raman system was set with 1800 lines/mm grating, exposure time 60 s (3 times), confocal hole of 100 μm and slit of 100 μm . The calibration was done using the main Raman line (520.5 cm^{-1}) of a silicon standard.

The Raman spectrum of the CaSiO_3 -walsstromite inclusion was collected at the Gemological Institute of America with a Renishaw inVia Raman microscope using the 514.5 nm output wavelength of a 150 mW argon-ion laser, at 100% output power. The analyses were performed using 50 \times LWD lens with a 0.55 numerical aperture and the system was set with 1800 lines/mm grating. Spectra were recorded in the frequency range extending from 100 to 1200 cm^{-1} ; to maximize the signal-to-noise ratio, each spectrum was collected four times using an exposure time of 60 s, and then merged together at the end of the acquisition. The calibration was done using an internal silicon standard (inside the instrument) using its main Raman line (520.5 cm^{-1}).

The baseline subtraction with a quadratic function and the Lorentzian fitting were carried out using the Thermo-Scientific OMNIC Spectra Software.

Ab initio calibration of CaSiO_3 -walsstromite Raman spectra at high pressure

The ab initio calculation of the vibrational frequencies and intensities of the Raman-active modes was performed by using the CRYSTAL14 software (Dovesi et al. 2014). A hybrid HF/DFT Hamiltonian was used (WC1LYP) that employs the Wu-Cohen DFT exchange functional (Wu and Cohen 2006) corrected with a fraction (20%) of the exact non-local Hartree-Fock exchange, and the Lee-Young-Parr DFT correlation functional (Lee et al. 1988). The grid for the evaluation of the DFT exchange-correlation functionals was chosen by the keyword XLGRID of the CRYSTAL14 user manual (Dovesi et al. 2014) and corresponds to a total of 345 185 points in the unit cell. A measure of the excellent numerical accuracy

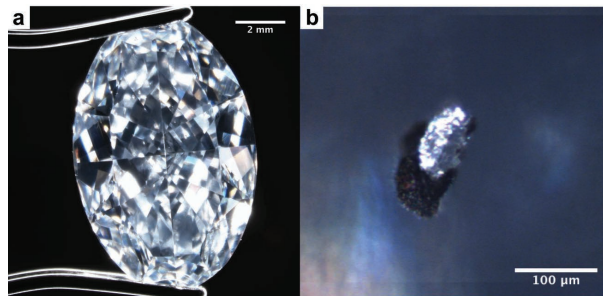


FIGURE 1. (a) Expanded view of the inclusion-bearing diamond studied in this work. (b) Close-up of the CaSiO_3 -walsstromite inclusion investigated. The black halo around the inclusion indicates the presence of graphitization inside a fracture. (Color online.)

provided by such a grid is the evaluation of the total number of electrons in the unit cell, by the numerical integration of the electron density over the cell volume: 348.000013 electrons out of 348. The atomic basis sets employed were from the CRYSTAL online library at the address www.crystal.unito.it/basis-sets.php. More precisely, they were 86-511G(2d) for Ca, 86-311G(1d) for Si, and 8-411G(2d) for O, where the symbols 1d and 2d stand for the presence of one and two polarization functions, respectively. The thresholds controlling the accuracy of the calculation of Coulomb and exchange integrals were set to 8 (ITOL1 to ITOL4) and 18 (Dovesi et al. 2014). The diagonalization of the Hamiltonian matrix was performed at 8 independent k vectors in the reciprocal space (Monkhorst net; Monkhorst and Pack 1976) by setting to 2 the shrinking factor IS (Dovesi et al. 2014). Cell parameters and fractional coordinates were optimized by analytical gradient methods, as implemented in CRYSTAL14 (Civalleri et al. 2001; Dovesi et al. 2014). Geometry optimization was considered converged when each component of the gradient (TOLDEG parameter in CRYSTAL14) was smaller than 0.00003 hartree/bohr and displacements (TOLDEX) were smaller than 0.00012 bohr with respect to the previous step. Lattice parameters and fractional coordinates were optimized at the WC1LYP level (static values: no zero point and thermal effects included), at the static pressures of 0 and 4 GPa, and at 4 other *non-hydrostatic* stress conditions specified by matrices representing the stress tensor in a Cartesian frame (with e_1 , e_2 , e_3 basis vectors), where the e_2 vector is parallel to the b lattice vector; the e_1 and e_3 vectors are, respectively, subparallel to the a and c lattice vectors, derived from a standard orthogonalization of the lattice basis. The chosen 4 stress matrices corresponded to a hydrostatic component of 4 GPa plus deviatoric stresses (pure shear, traceless stress matrices) having eigenvalues 1, -0.5 , and -0.5 GPa, and directions of maximum compression (eigenvalue 1 GPa), respectively, along e_1 , e_2 , e_3 , and the softest direction $[1\bar{1}2]$ (the latter one is given with reference to the crystal lattice basis). Vibrational frequencies were calculated at 0 and 4 GPa and at the four non-hydrostatic stress conditions, as the eigenvalues of the matrix of the second derivatives of the full potential of the crystal with respect to the mass-weighted nuclear displacements (Hessian matrix; Pascale et al. 2004). Relative intensities of the Raman signals are computed using a fully analytical approach formulated and implemented in the CRYSTAL14 program (Maschio et al. 2012, 2013).

RESULTS

Raman spectrum at ambient pressure

Before performing the high-pressure Raman measurements, we examined the Raman spectrum of the synthetic CaSiO_3 -walsstromite at ambient conditions (Fig. 2). The three main Raman peaks, in order of decreasing intensity, were observed at 656, 977, and 1037 cm^{-1} (hereafter called Peak 1, 2, and 3, respectively). The raw spectrum (Supplemental¹ Fig. S1) shows also lower intensity peaks in the 200–590 cm^{-1} region (the main ones at 301, 328, 349, 396, and 512 cm^{-1}) and in the 810–950 cm^{-1} region (the main ones at 813, 838, 857, and 950 cm^{-1}); another peak is centered at 1055 cm^{-1} . Our ambient Raman frequencies agree with those reported in previous studies within the experimental uncertainty (Nasdala et al. 2003; Brenker et al. 2005, 2007).

Effect of hydrostatic pressure on the Raman frequencies: Comparison between experiment and simulation

In situ Raman spectra of the three main peaks (656, 977, and 1037 cm^{-1}) of crystalline CaSiO_3 -walsstromite, measured as a function of pressure up to 7.5 GPa, are shown in Figure 2. Data analysis of the spectra was carried out using Thermo-Scientific OMNIC Spectra Software with Gaussian function. The measured frequencies are reported in Supplemental¹ Table 1.

It is evident that all Raman peaks shift continuously toward higher wavenumbers with increasing pressure throughout the pressure range. In particular, Peaks 1 and 2 show an almost linear trend. The pressure-dependence of the three main Raman bands was fitted with a weighted linear regression and the resulting pressure coefficients were: $dv/dP = 3.22(\pm 0.05) \text{ cm}^{-1} \text{ GPa}^{-1}$ for

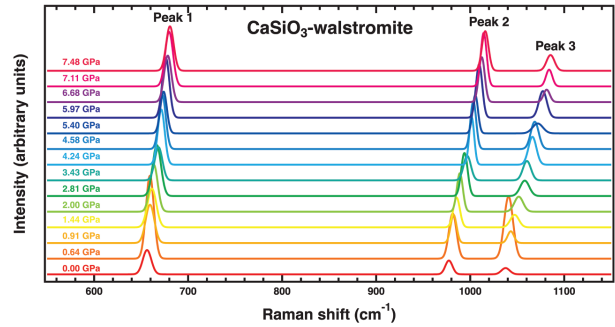


FIGURE 2. Raman spectra of synthetic CaSiO_3 -walsstromite up to 7.5 GPa. (Color online.)

Peak 1, $dv/dP = 5.16(\pm 0.09) \text{ cm}^{-1} \text{ GPa}^{-1}$ for Peak 2, and $dv/dP = 6.5(\pm 0.1) \text{ cm}^{-1} \text{ GPa}^{-1}$ for Peak 3 (Fig. 3a). Minor peaks were too weak to be fitted accurately at high pressure; therefore they were not considered for the calculation of the pressure coefficients.

Our calculated Raman spectra (Supplemental¹ Table 2) are comparable with the experimental frequencies reported in Supplemental¹ Table 1 within one or two standard deviations (σ). All Raman frequencies systematically increase with increasing pressure. The pressure dependence of the three main Raman bands was fitted with a weighted linear regression and the resulting pressure coefficients were: $dv/dP = 3.33 \text{ cm}^{-1} \text{ GPa}^{-1}$ for Peak 1, $dv/dP = 4.68 \text{ cm}^{-1} \text{ GPa}^{-1}$ for Peak 2, and $dv/dP = 5.90 \text{ cm}^{-1} \text{ GPa}^{-1}$ for Peak 3 (Fig. 3b). These pressure dependencies match well with the experimental ones within one or two standard deviations (σ).

Effect of non-hydrostatic pressure on the Raman frequencies

The ab initio calculated peak shifts under non-hydrostatic stresses show patterns similar to those under hydrostatic pressure (Fig. 4). Also, the pressure dependencies of the three main peaks under non-hydrostatic stresses are comparable to those calculated under hydrostatic pressure, the differences being less than 2σ (Table 1). Relative to the values under hydrostatic pressure, Peak 1 and Peak 3 show negative shifts under any non-hydrostatic stress state: the mean differences of the Δv are -1.4 cm^{-1} for Peak 1 and -1.0 cm^{-1} for Peak 3, which correspond to a mean difference of the ΔP of -0.5 and -0.19 GPa , respectively. Conversely, Peak 2 shows a negative shift when the maximum compression is along e_1 (i.e., subparallel to the a lattice vector) and e_3 (i.e., subparallel to the c lattice vector), but a positive shift when the maximum compression is along e_2 (i.e., parallel to the b lattice vector) and $[1\bar{1}2]$ (i.e., the softest direction, perpendicular to the layers): the mean difference of the Δv is -0.1 cm^{-1} , which corresponds to a mean difference of the ΔP of -0.02 GPa . This indicates that Peak 2 is the least sensitive to the application of differential stresses, and therefore it is the most reliable peak to be used as a calibrant to calculate the P_{inc} of a CaSiO_3 -walsstromite inclusion.

Inclusion residual pressure

The least sensitive peak to the deviatoric stress suffered by the CaSiO_3 -walsstromite inclusion enclosed in the diamond is

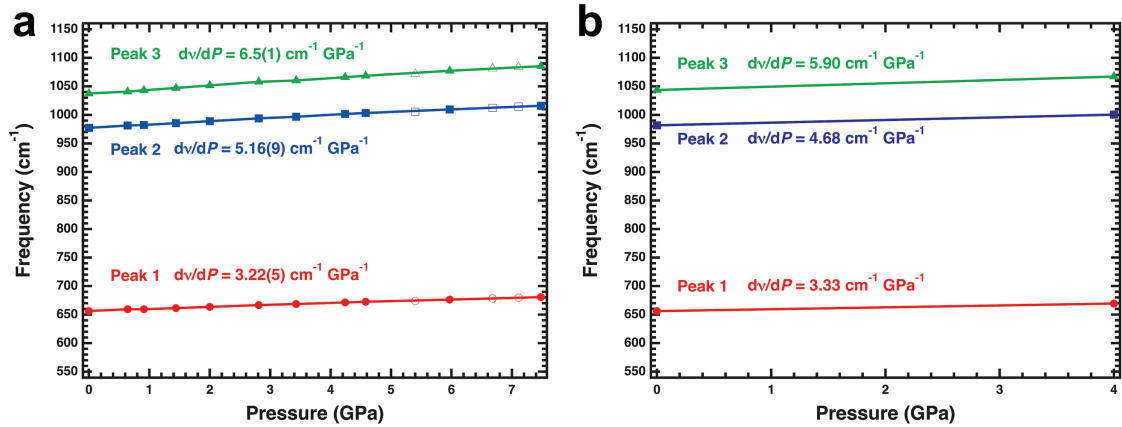


FIGURE 3. (a) Experimental and (b) calculated pressure-dependencies of the main Raman peaks of CaSiO_3 -walstromite under hydrostatic conditions. In a, compression and decompression are represented by solid and open symbols, respectively. The error bars lie within the symbols. (Color online.)

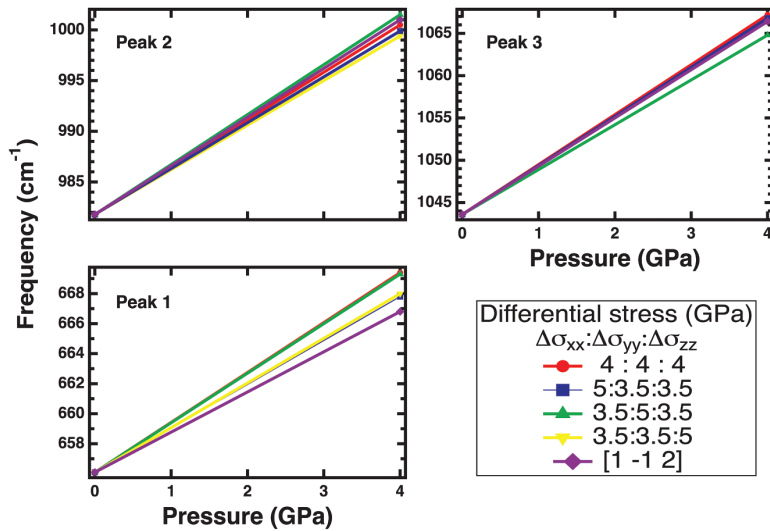


FIGURE 4. Calculated pressure dependencies of the three main Raman vibrational frequencies of CaSiO_3 -walstromite at different stress states. (Color online.)

Peak 2, as explained in the previous paragraph. For this reason, we used the experimental pressure coefficient for Peak 2, which is $5.16(\pm 0.09) \text{ cm}^{-1} \text{ GPa}^{-1}$, to calculate the residual pressure (P_{inc}) retained by the CaSiO_3 -walstromite inclusion found in the natural diamond (Fig. 1). The main Raman peaks of that inclu-

sion were observed at 669, 999, and 1061 cm^{-1} (Fig. 5), which are the highest frequencies ever reported in literature for a CaSiO_3 -walstromite still trapped within its diamond host. The calculation lead to the following residual pressure: $4.26(\pm 0.07) \text{ GPa}$.

DISCUSSION

The Raman measurements show that the CaSiO_3 -walstromite inclusion retains a residual pressure, as a consequence of the difference between the thermoelastic properties of the diamond host and those of the CaSiO_3 -walstromite inclusion. This residual pressure, measured at ambient conditions, can be used to calculate the entrapment pressure and temperature conditions of the host-inclusion pair, provided that the equations of state of the mineral phase and the diamond are known and reliable. The basic concept behind this approach is that, at

the moment of entrapment, the host fits the inclusion perfectly and the two are under the same P and T conditions (Izraeli et al. 1999; Howell et al. 2012; Nestola et al. 2012; Angel et al. 2014b, 2015b). However, this method relies on some assumptions: (1) the inclusion is spherical (Eshelby 1957, 1959; Mazzucchelli et al. 2017); (2) both the host and inclusion are elastically isotropic and homogeneous (Angel et al. 2014b); (3) at the moment of formation the inclusion perfectly fits in the diamond; and (4) deformation of

TABLE 1. Calculated shifts of Raman frequencies under hydrostatic and non-hydrostatic stresses

State of stress	Peak 1				Peak 2				Peak 3			
	ν (cm^{-1})	$\Delta\nu$ (cm^{-1})	$d\nu/dP$ ($\text{cm}^{-1}/\text{GPa}$)	ΔP (GPa)	ν (cm^{-1})	$\Delta\nu$ (cm^{-1})	$d\nu/dP$ ($\text{cm}^{-1}/\text{GPa}$)	ΔP (GPa)	ν (cm^{-1})	$\Delta\nu$ (cm^{-1})	$d\nu/dP$ ($\text{cm}^{-1}/\text{GPa}$)	ΔP (GPa)
Hydrostatic	669.4	–	3.33	–	1000.5	–	4.68	–	1067.2	–	5.90	–
Non-hydrostatic along e_1	667.8	–1.6	2.93	–0.5	999.9	–0.6	4.53	–0.13	1066.8	–0.4	5.80	–0.07
Non-hydrostatic along e_2	669.3	–0.1	3.30	0.0	1001.5	1.0	4.93	0.21	1064.8	–2.4	5.30	–0.45
Non-hydrostatic along e_3	668.0	–1.4	2.98	–0.5	999.4	–1.1	4.40	–0.26	1066.5	–0.7	5.73	–0.11
Non-hydrostatic along $[1\bar{1}2]$	666.8	–2.6	2.68	–1.0	1001.0	0.5	4.80	0.10	1066.4	–0.7	5.70	–0.12
	$\Delta\nu$	–1.4	ΔP	–0.5	$\Delta\nu$	–0.1	ΔP	–0.02	$\Delta\nu$	–1.0	ΔP	–0.19

Notes: Differences $\Delta\nu$ and ΔP are with respect to the hydrostatic value. Positive values mean shift toward higher frequencies, negative values mean shift toward lower frequencies. $\Delta\nu$ and ΔP are the mean difference of the frequency and of the pressure, respectively, evaluated over the set of total numbers of peaks.

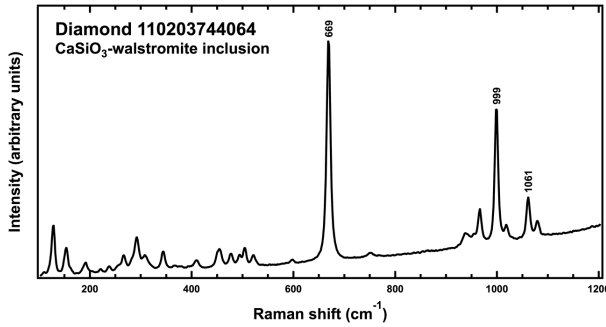


FIGURE 5. Raman spectrum of the CaSiO_3 -walstromite inclusion found in the natural diamond.

both the host and the inclusion is elastic and no brittle or plastic deformation has occurred. The assumption that both the host and the inclusion are elastically isotropic implies that the inclusion is under isotropic strains. But the stress state in an anisotropic inclusion subject to isotropic strains (e.g., there is no fluid at the interface, see Nimis et al. 2016) such as CaSiO_3 -walstromite is never hydrostatic (Anzolini et al. 2016) and, therefore, its Raman shifts may potentially be affected by such non-isotropic deformation. Nevertheless, our results indicate that the second highest peak of CaSiO_3 -walstromite, located at 977 cm^{-1} , is not very sensitive to non-hydrostatic stress, being the mean difference of the ΔP with respect to the hydrostatic value only -0.02 GPa (see Table 1), and thus it is suitable to estimate the remnant pressure of a CaSiO_3 -walstromite inclusion within a negligible error.

The calculation of the pressure of formation (P_c) for the CaSiO_3 -walstromite–diamond pair was performed with the software EoSFit7c (Angel et al. 2014a), by following the same method described in Angel et al. (2014b). We used thermal expansion and compressibility data for CaSiO_3 -walstromite reported in Anzolini et al. (2016), thermoelastic properties for diamond from the review of Angel et al. (2015a) and the residual pressure obtained in this work, which is $4.26(\pm 0.07)\text{ GPa}$.

Assuming a temperature range between 1200 and 2000 K for CaSiO_3 -walstromite formation (i.e., the same temperature range at which CaSiO_3 -walstromite was successfully synthesized by Gasparik et al. 1994), we obtained entrapment pressures ranging from 8.10 to 9.27 GPa [$P_{\text{inc}} = 4.26(\pm 0.07)\text{ GPa}$] (Supplemental Table 3), corresponding to 240–280 km depth (Fig. 6). Such pressure can be considered as a minimum estimate because of the presence of cracks around the inclusion (Fig. 1b), which would partly release the stress (see Mazzucchelli et al. 2016) and the effect of plastic deformation of diamond, which, if present, is not quantifiable yet. Taking this into consideration, the entrapment pressure could be set at higher values, at least on the boundary between CaSiO_3 -walstromite and larnite + CaSi_2O_5 -titanite. Considering instead Peak 1 or Peak 3 with the hydrostatic calibration, the arising error in the entrapment pressure would be ~ 0.5 and $\sim 0.9\text{ GPa}$, respectively, corresponding to an underestimation of the depth of about 10–20 km.

IMPLICATIONS

Our results on CaSiO_3 -walstromite indicate that the main Raman peaks of CaSiO_3 -walstromite are sensitive to deviatoric

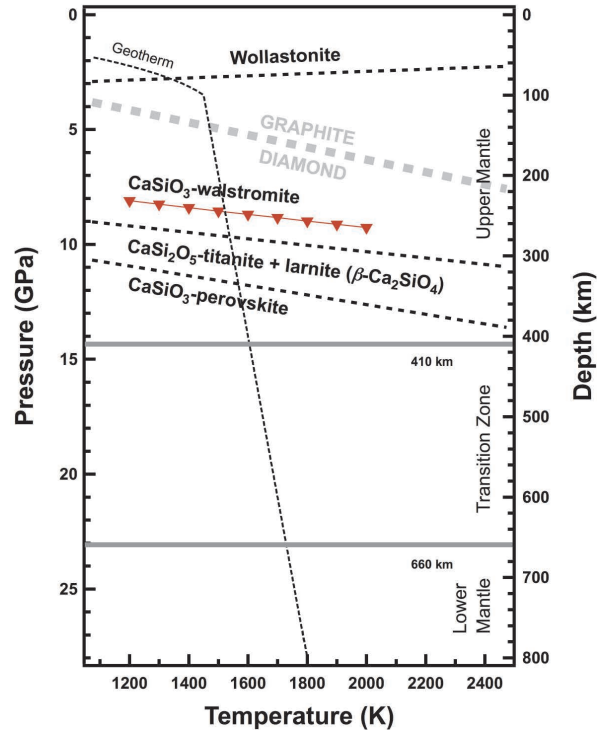


FIGURE 6. Phase diagram of the CaSiO_3 system, in which the phase boundaries are given as dotted lines (Essene 1974; Gasparik et al. 1994). The graphite–diamond phase boundary is shown as a gray dashed line (Day 2012). The geotherm is shown as a black dashed line (Turcotte and Schubert 2014). The 410 and 660 km discontinuities enclosing the transition zone are indicated by bold lines. Entrapment pressures from which our sample may have originated are represented with red symbols. (Color online.)

stress, with Peak 1 (656 cm^{-1}) and Peak 2 (977 cm^{-1}) showing the largest and smallest shifts, respectively. As a general rule, the use of these peaks is not ideal to retrieve reliable pressures from the Raman shifts. On the other hand, Peak 2, being the least sensitive to deviatoric stresses can be used, as in the present study, to calibrate the residual pressure retained by a CaSiO_3 -walstromite inclusion still trapped in a diamond within a negligible error. Through this approach, we estimate the formation depth of a diamond– CaSiO_3 -walstromite pair to be $P \sim 9\text{ GPa}$ ($\sim 260\text{ km}$) if the temperature is 1800 K. This can be considered as a minimum value, as the presence of fractures at the diamond–inclusion interface would partly release the internal pressure of the inclusion. These results suggest that the diamond investigated is certainly sub-lithospheric and endorse the hypothesis that the presence of CaSiO_3 -walstromite is a strong indication of super-deep origin.

ACKNOWLEDGMENTS

This investigation was financially supported by Fondazione Cassa di Risparmio di Padova e Rovigo and by the project INDIMEDEA, funded by the ERC-StG 2012 to F.N. (Grant No. 307322). M.A. has been supported by the Italian SIR-MIUR MILE DEEp (Grant No. RBS1140351) and the ERC-StG 2016 TRUE DEPTHS (Grant No. 714936). Ross J. Angel is thanked for advice and discussion. We are also grateful to H.M. Lamadrid for reviewing the manuscript.

REFERENCES CITED

- Angel, R.J., Alvaro, M., and Gonzalez-Platas, J. (2014a) EosFit7c and a Fortran module (library) for equation of state calculations. *Zeitschrift für Kristallographie-Crystalline Materials*, 229, 405–419.
- Angel, R.J., Mazzucchelli, M.L., Alvaro, M., Nimis, P., and Nestola, F. (2014b) Geobarometry from host-inclusion systems: The role of elastic relaxation. *American Mineralogist*, 99, 2146–2149.
- Angel, R.J., Alvaro, M., Nestola, F., and Mazzucchelli, M.L. (2015a) Diamond thermoelastic properties and implications for determining the pressure of formation of diamond-inclusion systems. *Russian Geology and Geophysics*, 56, 211–220.
- Angel, R.J., Nimis, P., Mazzucchelli, M.L., Alvaro, M., and Nestola, F. (2015b) How large are departures from lithostatic pressure? Constraints from host-inclusion elasticity. *Journal of Metamorphic Geology*, 33, 801–813.
- Anzolini, C., Angel, R.J., Merlini, M., Derzsi, M., Tokár, K., Milani, S., Krebs, M.Y., Brenker, F.E., Nestola, F., and Harris, J.W. (2016) Depth of formation of CaSiO₃-walsstromite included in super-deep diamonds. *Lithos*, 265, 138–147.
- Artioli, G., Angelini, I., and Polla, A. (2008) Crystals and phase transitions in prothistoric glass materials. *Phase Transitions*, 81, 233–252.
- Brenker, F.E., Stachel, T., and Harris, J.W. (2002) Exhumation of lower mantle inclusions in diamond: ATEM investigation of retrograde phase transitions, reactions and exsolution. *Earth and Planetary Science Letters*, 198, 1–9.
- Brenker, F.E., Vincze, L., Vekemans, B., Nasdala, L., Stachel, T., Vollmer, C., Kersten, M., Somogyi, A., Adams, F., and Joswig, W. (2005) Detection of a Ca-rich lithology in the Earth's deep (>300 km) convecting mantle. *Earth and Planetary Science Letters*, 236, 579–587.
- Brenker, F.E., Vollmer, C., Vincze, L., Vekemans, B., Szymanski, A., Janssens, K., Szaloki, I., Nasdala, L., Joswig, W., and Kaminsky, F. (2007) Carbonates from the lower part of transition zone or even the lower mantle. *Earth and Planetary Science Letters*, 260, 1–9.
- Civalleri, B., D'Arco, P., Orlando, R., Saunders, V., and Dovesi, R. (2001) Hartree-Fock geometry optimisation of periodic systems with the CRYSTAL code. *Chemical Physics Letters*, 348, 131–138.
- Day, H.W. (2012) A revised diamond-graphite transition curve. *American Mineralogist*, 97, 52–62.
- Dovesi, R., Saunders, V., Roetti, C., Orlando, R., Zicovich-Wilson, C., Pascale, F., Civalleri, B., Doll, K., Harrison, N., and Bush, I. (2014) CRYSTAL14 User's Manual. University of Torino, Italy.
- Eshelby, J.D. (1957) The determination of the elastic field of an ellipsoidal inclusion, and related problems. In *Proceedings of the Royal Society of London A: Mathematical, Physical and Engineering Sciences*, 376–396. The Royal Society.
- (1959) The elastic field outside an ellipsoidal inclusion. In *Proceedings of the Royal Society of London A: Mathematical, Physical and Engineering Sciences*, 561–569. The Royal Society.
- Essene, E. (1974) High-pressure transformations in CaSiO₃. *Contributions to Mineralogy and Petrology*, 45, 247–250.
- Frost, D.J. (2008) The upper mantle and transition zone. *Elements*, 4, 171–176.
- Gasparik, T., Wolf, K., and Smith, C.M. (1994) Experimental determination of phase relations in the CaSiO₃ system from 8 to 15 GPa. *American Mineralogist*, 79, 1219–1222.
- Harte, B. (2010) Diamond formation in the deep mantle: the record of mineral inclusions and their distribution in relation to mantle dehydration zones. *Mineralogical Magazine*, 74, 189–215.
- Howell, D., Wood, I.G., Nestola, F., Nimis, P., and Nasdala, L. (2012) Inclusions under remnant pressure in diamond: a multi-technique approach. *European Journal of Mineralogy*, 4, 563–573.
- Irfune, T., and Ringwood, A. (1987) Phase transformations in a harzburgite composition to 26 GPa: implications for dynamical behaviour of the subducting slab. *Earth and Planetary Science Letters*, 86, 365–376.
- Izraeli, E., Harris, J., and Navon, O. (1999) Raman barometry of diamond formation. *Earth and Planetary Science Letters*, 173, 351–360.
- Joswig, W., Stachel, T., Harris, J.W., Baur, W.H., and Brey, G.P. (1999) New Ca-silicate inclusions in diamonds—tracers from the lower mantle. *Earth and Planetary Science Letters*, 173, 1–6.
- Kaminsky, F. (2012) Mineralogy of the lower mantle: A review of “super-deep” mineral inclusions in diamond. *Earth-Science Reviews*, 110, 127–147.
- Lee, C., Yang, W., and Parr, R.G. (1988) Development of the Colle-Salvetti correlation-energy formula into a functional of the electron density. *Physical Review B*, 37, 785.
- Mao, H., Xu, J., and Bell, P. (1986) Calibration of the ruby pressure gauge to 800 kbar under quasi-hydrostatic conditions. *Journal of Geophysical Research: Solid Earth*, 91, 4673–4676.
- Maschio, L., Kirtman, B., Orlando, R., and Rérat, M. (2012) Ab initio analytical infrared intensities for periodic systems through a coupled perturbed Hartree-Fock/Kohn-Sham method. *The Journal of Chemical Physics*, 137, 204113.
- Maschio, L., Kirtman, B., Rérat, M., Orlando, R., and Dovesi, R. (2013) Ab initio analytical Raman intensities for periodic systems through a coupled perturbed Hartree-Fock/Kohn-Sham method in an atomic orbital basis. I. Theory. *The Journal of Chemical Physics*, 139, 164101.
- Mazzucchelli, M.L., Angel, R.J., Rustioni, G., Milani, S., Nimis, P., Domeneghetti, M.C., Marone, F., Harris, J.W., Nestola, F., and Alvaro, M. (2016) Elastic geobarometry and the role of brittle failure on pressure release. In *EGU General Assembly Conference Abstracts*, 13569.
- Mazzucchelli, M.L., Burnley, P.C., Angel, R.J., Domeneghetti, M.C., Nestola, F., and Alvaro, M. (2017) Elastic geobarometry: uncertainties arising from the geometry of the host-inclusion system. In *EGU General Assembly Conference Abstracts*, 2060.
- Milani, S., Nestola, F., Angel, R., Nimis, P., and Harris, J. (2016) Crystallographic orientations of olivine inclusions in diamonds. *Lithos*, 265, 312–316.
- Monkhorst, H.J., and Pack, J.D. (1976) Special points for Brillouin-zone integrations. *Physical Review B*, 13, 5188.
- Nasdala, L., Brenker, F.E., Glinnemann, J., Hofmeister, W., Gasparik, T., Harris, J.W., Stachel, T., and Reese, I. (2003) Spectroscopic 2D-tomography Residual pressure and strain around mineral inclusions in diamonds. *European Journal of Mineralogy*, 15, 931–935.
- Nestola, F., Merli, M., Nimis, P., Parisatto, M., Kopylova, M., De Stefano, A., Longo, M., Ziberna, L., and Manghni, M. (2012) In situ analysis of garnet inclusion in diamond using single-crystal X-ray diffraction and X-ray microtomography. *European Journal of Mineralogy*, 24, 599–606.
- Nestola, F., Nimis, P., Angel, R., Milani, S., Bruno, M., Precipice, M., and Harris, J. (2014) Olivine with diamond-imposed morphology included in diamonds. Syngeneisis or protogeneisis? *International Geology Review*, 56, 1658–1667.
- Nestola, F., Burnham, A.D., Peruzzo, L., Tauro, L., Alvaro, M., Walter, M.J., Gunter, M., Anzolini, C., and Kohn, S.C. (2016) Tetragonal Almandine-Pyrope Phase, TAPP: finally a name for it, the new mineral jeffbenite. *Mineralogical Magazine*, 80, 1219–1232.
- Nestola, F., Jung, H., and Taylor, L.A. (2017) Mineral inclusions in diamonds may be synchronous but not syngenetic. *Nature Communications*, 14168.
- Nimis, P., Alvaro, M., Nestola, F., Angel, R.J., Marquardt, K., Rustioni, G., Harris, J.W., and Marone, F. (2016) First evidence of hydrous silicic fluid films around solid inclusions in gem-quality diamonds. *Lithos*, 260, 384–389.
- Pascale, F., Zicovich-Wilson, C.M., Lopez-Gejo, F., Civalleri, B., Orlando, R., and Dovesi, R. (2004) The calculation of the vibrational frequencies of crystalline compounds and its implementation in the CRYSTAL code. *Journal of Computational Chemistry*, 25, 888–897.
- Pearson, D., Brenker, F., Nestola, F., McNeill, J., Nasdala, L., Hutchison, M., Matveev, S., Mather, K., Silversmit, G., and Schmitz, S. (2014) Hydrous mantle transition zone indicated by ringwoodite included within diamond. *Nature*, 507, 221–224.
- Ringwood, A. (1991) Phase transformations and their bearing on the constitution and dynamics of the mantle. *Geochimica et Cosmochimica Acta*, 55, 2083–2110.
- Stachel, T., and Harris, J. (2008) The origin of cratonic diamonds—constraints from mineral inclusions. *Ore Geology Reviews*, 34, 5–32.
- Turcotte, D., and Schubert, G. (2014) *Geodynamics*, 3rd ed. Cambridge University Press.
- Van der Molen, I., and Van Roermund, H. (1986) The pressure path of solid inclusions in minerals: the retention of coesite inclusions during uplift. *Lithos*, 19, 317–324.
- Wu, Z., and Cohen, R.E. (2006) More accurate generalized gradient approximation for solids. *Physical Review B*, 73, 235116.

MANUSCRIPT RECEIVED MAY 8, 2017

MANUSCRIPT ACCEPTED SEPTEMBER 25, 2017

MANUSCRIPT HANDLED BY MAINAK MOOKHERJEE